Performance Limitations of Varactor Multipliers*

Jack East
Center for Space Terahertz Technology, The University of Michigan
Erik Kollberg
Chalmers University of Technology
Margaret Frerking
NASA/JPL

ABSTRACT

Large signal nonlinear device circuit modeling tools are used to design varactor harmonic multipliers for use as millimeter and submillimeter wave local oscillator pump sources. The results predicted by these models are in reasonable agreement with experimental results at lower frequencies, but the agreement becomes worse as the power level or frequency increases. We will discuss an improved varactor device model and compare results from the new model with both conventional models and experimental data.

I. Introduction

The Schottky barrier varactor frequency multiplier is a critical component of millimeter wave and submillimeter wave receiver systems. A variety of modeling tools are available to help in the design of the multipliers. The modeling is a combination of linear and nonlinear analysis to find the current and voltage waveforms across the varactor placed in the multiplier circuit. The conventional approach uses the harmonic balance[1,2] or multiple reflection technique[3]. These techniques start with a time domain approximation for the voltage across the device and time domain information for the nonlinear device and frequency domain information from the linear circuit to find the final waveforms across the device. These techniques are available in many commercial circuit simulators[1,2] and in more specialized mixer programs[3–5].

These techniques require an equivalent circuit to describe the varactor. Measured or calculated information on the capacitance and current vs. voltage can be used. The multiplier performance also depends on the series resistance of the device. This is more difficult to obtain from low frequency measurements, so a variety of approximations are used. These techniques have been used to design multipliers over a wide range of frequencies. The results are encouraging at lower frequencies. However, as the frequency or power level goes up the predicted powers and efficiencies are typically lower than experimental results. There are several possible explanations. High frequency multiplier circuits are small and difficult to fabricate. Skin effect and backshort loss both increase with frequency. These losses can be taken into account in the simulation, but the required

*This work was supported by the Center for Space Terahertz Technology under contract No. NAGW-1334.

loss values tend to be relatively large when compared with other information about waveguide and mount loss. The impedance presented to the device by the circuit is sometime inferred from scale model measurements at much lower frequencies. As the operating frequency increases mechanical tolerance limitations make it more difficult to predict the operating conditions from scale models. Another problem is the varactor diodes themselves. There are a limited number of varactor designs at high frequencies, so scaling over frequency is difficult. Another problem is the equivalent circuit used to describe the nonlinear varactor. At high frequencies or power levels, a simple lumped element equivalent circuit can have problems representing the actual operation of the varactor. A recent paper by Kollberg et al[6] described saturation effects in varactors using a lumped element representation for the varactor with elements that depended on the current level. That paper is the starting point for the present work.

We will discuss a varactor model in this paper that takes the device physics into account in more detail, and then use the proposed new model to study multiplier performance. The next section of the paper describes the details of the new model. Section 3 will discuss the results of including the new effects on the performance of a multiplier operating between 80 and 160 GHz. The paper will be summarized in section 4.

II. Improved Varactor Model

There are two extremes in device models; analytic or equivalent circuit models that are used in a variety of circuit simulators like SPICE and the nonlinear models discussed in the introduction, and more complete semiconductor models that solve for the internal physics in more detail. These more complete models typically solve a combination of the time dependent current continuity and Poissons' equation to find the terminal characteristics of the device. This type of solution is commonly used for IMPATT diodes[7,8] and Gunn devices[9,10]. Problems occur when a detailed numerical model is connected to a nonlinear circuit simulation to study harmonic multiplication. The time scale of the circuit simulation is some fraction of an RF period, typically picoseconds. The time scale of the semiconductor simulation is on the order of the dielectric relaxation time, which is femtoseconds. The computer time required to time step through an RF cycle is much larger than in the conventional equivalent circuit case. We propose an alternative model that includes most of the varactor physics to better understand the operation, but can be used in a nonlinear algorithm with reasonable amounts of computer time.

An improved varactor model can be found by first studying the operation of a typical varactor diode using a drift-diffusion semiconductor simulation. This simulation solves the electron current continuity equation and Poissons' equation as a function of time and position to describe the terminal characteristics of a varactor diode. The diode is 0.6 microns long and is doped at $3\times10^{16}/\mathrm{cm}^3$, similar to the experimental device in section III. The results of a two volt switching transient are shown in Fig. 1. The width of the depletion layer increases by removing electrons from the depletion layer edge and out of

the device. This is shown in Fig. 1a. The resulting electric field as a function of time is shown in Fig. 1b. The voltage step at the start of the transient produces a modified electric field inside the device. For very short times the electrons in the device can not rearrange themselves. The effect of the voltage increase is to increase the field in the entire device by an amount

$$\Delta E = \Delta V/\text{width}. \tag{1}$$

The two volt step produces a 33 KV/cm field increase across the entire device. The field increases in the depletion region where the electron density is small, and also in the undepleted region where the electron density is large. Since the electron density in the undepleted region is approximately constant the field produces an electron conduction current of

$$J_n = q \times n \times v_n(E), \tag{2}$$

where

J_n = electron current,
n = electron density,
v_n(E) = electron velocity,
E = electric field.

The particle current in the undepleted region and the displacement current in the depletion region as a function of time are shown as solid lines in Fig. 2. The first difference between the semiconductor model and an equivalent circuit model occurs as a result of equation 2. Most varactor models include a voltage dependent capacitance and a constant or voltage variable series resistance. The result of a switching transient would be an exponential decay of current with time, with a small variation due to the changing depletion layer capacitance. However, for the results in Fig. 2, the current depends on the electric field, and both the velocity and the current are limited to peak values by the semiconductor physics. The electric field in the entire device is above the saturation field at the start of the transient. Since the electron momentum relaxation time or the time required to reach the equilibrium vilocity is much shorter than the time scale under consideration, all the electrons are moving at the saturated velocity. The electron current changes slowly during the first 1.5 picoseconds of the transient because of this saturation. The electron current in Fig. 2 is caused by electrons exiting the device and increasing the depletion layer width. This electron motion changes the electric field distribution within the device and supports displacement current in the depletion layer. The field profiles vs. time in Fig. 1 show the effect of the electron redistribution. The field at the Schottky contact becomes larger (more negative) and the field at the ohmic contact becomes smaller (less negative) during the transient. The resulting time change in the field produces the current vs. time information shown in Fig. 2. Fig. 2 points out a second difference with the lumped circuit models. The total current at any point in the device is the sum of the particle and displacement currents, and is constant with position and varies with time. The difference between the displacement current in the depletion region and the electron current in the undepleted region is accounted for by displacement current in the otherwise resistive portion of the device, shown as curve c. The changing electric field in the undepleted region supports this displacement current. The time scale

and voltage change in Figs. 1 and 2 are similar to the picosecond time scale and several volts RF level associated with multipliers operating above 100 GHz. The results show the importance of the displacement current and velocity saturation. However a typical reflection algorithm goes through many RF periods in the course of a solution and the computer time required to combine this exact description with the nonlinear solution quickly becomes excessive. We will discuss a simple model that includes many of these saturation effects next.

The information from the complete semiconductor model discussed in the last paragraph can be used as a starting point for a numerically efficient varactor model. The model uses a combination of the depletion layer approximation and equation 2 to describe the device. The voltage drop associated with the depletion region is

$$V_{dep} = q \times N_d \times W_{dep}/2\epsilon, \tag{3}$$

where V_{dep} = depletion layer voltage,
N_d = doping and,
W_{dep} = depletion layer width.
W_{dep} at the start of a transient is dependent on the initial voltage across the device and the built-in barrier potential, and changes as a result of electron current in the device. When a voltage step is applied, W_{dep}, V_{dep} and J_n can be found by using equations 2 and 3 along with an expression for the field in the neutral region,

$$E = -(V_{terminal} + V_{bi} - V_{dep})/x_{total}, \tag{4}$$

where $V_{terminal}$ = external voltage from the circuit,
V_{bi} = built-n potential, and
x_{total} = overall device epitaxial length.
These three equations can be solved as a function of time and terminal voltage to produce the varactor current waveform. These equations have most of the characteristics of the more complete semiconductor model, but run in a small fraction of the computer time. The transient results predicted by these three equations are shown as dashed lines in Fig. 2.

The model described in the last paragraph is an ideal varactor. However, with a large enough voltage swing, the device can conduct in the forward direction if the junction is forward biased and conduct in the reverse direction if the voltage is above the breakdown voltage. These two currents should be included in the model. The forward current can be approximated by a thermionic emission current that depends on the voltage across the depletion layer inside the device

$$I_{th} = A \times A^* T^2 \exp(-V_{dep}/kT), \tag{5}$$

where A = area,
A* = Richardson's constant, and

T = temperature.

Under moderate voltage low frequency conditions, the depletion layer voltage is close to the terminal voltage. As the forward voltage increases, the thermionic current increases and a portion of the terminal voltage drops in the undepleted region. This voltage drop limits the forward current and device capacitance, even for terminal voltages beyond flatband. Under high frequency operation, the undepleted region must support both the forward junction current and the junction displacement current. This will further limit the current. The current and voltage waveforms predicted using a lumped element varactor model in a nonlinear simulator can swing the device beyond the measured DC breakdown voltage. Breakdown effects need to be included in the varactor model. A detailed description of breakdown effects is given by Sze[11]. The ionization current is small for reverse bias voltages below the breakdown voltage and increases rapidly above the breakdown voltage. The breakdown current can be modeled as a current generator that depends on the voltage above the breakdown voltage. The ionization current will flow through the depletion layer and be limited by the space charge resistance, (equation 12 page 214 in Sze[11])

$$R_{space\ charge} = W_{dep}^2/(2 \times A\epsilon \times v_{sat}), \tag{6}$$

where

v_{sat} = saturated velocity in the depletion layer.

The avalanche current becomes

$$\begin{aligned} I_{avalanche} &= 0 \text{ if } V_{dep} < V_{breakdown}, \text{ and} \\ &= A^*(V_{dep} - V_{breakdown})/R_{space\ charge} \text{ otherwise.} \end{aligned} \tag{7}$$

This avalanche current will also flow through the undepleted region of the device and will have the same saturation effects as the other currents under consideration. This expression for the avalanche current neglects time delays associated with the avalanche response time and transit time effects in the depletion layer.

A varactor model that includes the current effects in equations 2, 5 and 7 along with the depletion layer effects in equations 3 and 4 has been written and interfaced to a modified version of the program DIODEMX described by Maas[5]. The combined varactor and nonlinear multiplier program has been used to study doubler performance.

Section III. Multiplier Performance

The varactor effects discussed in the last section have been included in a multiple reflection multiplier program to study the performance of a doubler operating between 90 and 180 GHz. The varactor parameters and operating conditions have been chosen to match an experimental doubler discussed by Erickson[12] to allow comparison with experimental data. The varactors have a doping of $3\times10^{16}/cm^3$, two devices with an area of $38\times10^{-8}cm^2$ each, a series resistance of 10 ohms and a breakdown voltage of 20 volts. The solutions were found at the experimental bias points that were obtained from Erickson[13] and Raissanen[14].

Fig. 3 shows the experimental efficiency and the predicted efficiency for a conventional diode model. Curve (a) is the measured efficiency. The estimated output circuit loss was 1.3 dB. Curve (b) is the estimated power generated at the device with the output loss removed. Curve (c) is the output efficiency predicted by the conventional varactor model. The simple varactor model does a reasonable job of predicting the multiplier performance at low power levels, but has problems for pump powers above 30 milliwatts. The various effects discussed above can be included to better understand this difference.

The effects of current saturation can be included in the varactor program by using equations 2, 3, 4, 5 and 7 to describe the device performance. The model requires an expression for the velocity vs. electric field in equation 2. A simple expression for velocity vs. field has a constant low field mobility at low electric fields and a constant saturated velocity at higher fields. The choice of mobility and saturated velocity values will effect the performance predictions. The simplest velocity vs. field expression is a constant mobility with no velocity saturation effects included. Except for a modulation of the series resistance because of a modulation of the undepleted layer width, this varactor approximation is the same as the conventional model. The resulting efficiency vs. local oscillator power is shown in Fig. 4 for mobilities between 3000 and 6000 cm^2/Volt-sec. Since breakdown and current saturation effects are not included, the efficiencies have the same monotonic increase as the data in Fig. 3. Based on the device dimensions, doping and experimental low frequency series resistance, the estimated experimental mobility is 4000 to 4500 cm^2/Volt-sec. The best approximation to the experimental data below about 35 milliwatts pump power is the 3000 cm^2/Volt-sec data, a lower than expected result. One possible explanation is a frequency dependent series resistance due to the change in skin depth with frequency. This difference can also be explained by including displacement current in the varactor model.

There is displacement current flowing through the entire length of the varactor during its operation. This bulk displacement current is a small fraction of the electron current, but it is usually of the opposite sign. The effect of the displacement current on the efficiency vs. pump power level is shown in Fig. 5. The efficiencies in Fig. 5 are lower than the corresponding efficiencies in Fig. 4. A low field mobility of 4500 cm^2/Volt-sec gives a match to the experimental data, and is also reasonable when compared with the low frequency series resistance.

The model parameters in Fig. 5 do a good job of predicting the low power performance of the multiplier, and the choice of a low field mobility of 4500 cm^2/Volt-sec is a good match to both the RF data and the measured low frequency series resistance. However, the model efficiency still has a monotonic increase with power level while the experimental data efficiency decreases above about 40 milliwatts pump power. The next step is to include velocity saturation effects in the model. Figure 6 shows the efficiency vs. pump power for saturated velocities between 2.5×10^7 and 4×10^7cm/sec. All the curves show the saturation effects of the experimental data. The effect of the finite saturated velocity is to limit the maximum conduction current through the device. This in turn limits the

rate of change of the depletion layer with and thus the nonlinear capacitance. circuit. Reducing the saturated velocity reduces the electric field and pump power required to saturate the device. The saturation point for the curves in Fig. 6 varies between about 30 milliwatts for the lowest velocity(curve d) to about 60 milliwatts for the highest velocity(curve a). A saturated velocity of 3.5×10^7cm/sec gives a reasonable fit to the experimental data.

The best fit velocity in Fig. 6 is higher than the typical measured saturation velocity in GaAs. However, the measured velocity characteristic are based on DC measurements of long samples. Velocity saturation occurs in GaAs because of electron heating and valley transfer. Valley transfer only occurs when the electrons obtain a minimum threshold energy. In the varactor structure the distances are small and the field is changing rapidly. As a check on the solution, the voltage drop in the undepleted portion of the varactor was displayed. Although the electric field was high, the maximum voltage drop in the undepleted region was below the valley transfer threshold in GaAs for all the cases in Fig. 6. Thus a velocity vs. electric field based on central valley transport with a high saturated velocity is reasonable.

The effects of undepleted region displacement current and velocity saturation account for most of the reduction in efficiency for low and medium pump power levels. However, the device is biased past the breakdown voltage for higher pump levels. The effect of adding the breakdown current to the model of Fig. 6 is shown in Fig. 7. The three dashed curves correspond to source resistances of 800, 1000 and 1200 ohms. The model also includes the displacement current and velocity saturation effects. The device is pumped past the breakdown voltage for pump power levels above 40 to 50 milliwatts. The peak voltage across the device when breakdown effects are not included is about 34 volts. Including breakdown effects lowers the peak voltage to about 26 volts. The reduced voltage swing reduces the capacitance swing and the nonlinearity of the junction capacitance. The breakdown also adds an in- phase current to the total device current. The combined effect is a lower efficiency at higher pump power levels.

IV. Conclusions

This paper has discussed the large signal nonlinear modeling of varactor multipliers. Earlier multiplier models have used a lumped element voltage dependence model to describe the varactor. This approach does not match the experimental results at higher frequencies and power levels. This paper has described a new varactor model more closely based on the semiconductor device operation. Three effects in the new model modify the varactor and multiplier performance. At low pump power levels the changing electric field in the undepleted portion of the device produces a displacement current. This current reduces the low power efficiency. At medium pump power levels the electron velocity begins to saturate and an additional reduction in efficiency occurs. The total voltage drops in the undepleted region are small, so the velocity characteristics depend on the properties of central valley electrons in the GaAs. For higher pump powers the varactor

voltage is above the breakdown voltage and avalanche current flows. This further reduces the efficiency. The model was tested for a range of material and device parameters and compared with experimental data. The parameters needed to match the experimental results are all physically reasonable.

Acknowledgments: The authors would like to thank Dr. Neal Erickson and Dr. Antti Raissanen for useful discussions and for unpublished experimental information on experimental multiplier performance.

List of Figures

References

1. *LIBRA Users Guide*, EESOF, 5601 Lindero Canyon Road, Westlake Village, California, 91362.

2. Compact Software, 483 McLean Blvd., Patterson, New Jersey, 07504.

3. A. R. Kerr, "A Technique for Determining the Local Oscillator Waveform in a Microwave Mixer," *IEEE Trans. on Microwave Theory and Techniques*, volume MTT-23, 1975, p. 828.

4. P. Siegel, A. Kerr and W. Hwang, "Topics in the Optimization of Millimeter Wave Mixers," NASA Technical Paper 2287, March, 1984.

5. S. Maas, *Microwave Mixers,* Artech House, Norwood, Mass. 1986, chapter 4 and appendix A.

6. E. L. Kollberg, T. J. Tolmunen. M. A. Frerking and J. R. East, "Current Saturation in Submillimeter Wave Varactors," *IEEE Trans. on MTT,* volume MTT-40, 1992, p. 831-838.

7. D. L. Scharfetter and H. K. Gummel, "Large Signal Analysis of a Silicon Read Diode Oscillator," *IEEE Trans. on Electron Devices*, volume ED-16, pp. 64, 1969.

8. W. E. Schroeder and G. I. Haddad, "Nonlinear Properties of IMPATT Devices," Proc. IEEE, vol. 61, pp 153, 1973.

9. J. A. Copeland, "A new mode od oscillation for bulk negative resistance oscillators," Proc. IEEE(letters), vol. 54, no. 10, pp. 1479- 1480, Oct. 1966.

10. D. D. Khandelwal and W. R. Curtice, "A study of the single-frequency quenched-domain mode Gunn-effect oscillator," *IEEE Trans. on Microwave Theory and Technique*, vol. MTT-18, no. 4, pp. 178-187, April, 1970.

11. S.M. Sze, *Physics of Semiconductor Devices,* Wiley, 2nd edition,1981.

12. N. Erickson, "High efficiency submillimeter frequency multipliers," 1990 IEEE S Int. Microwave Symposium Digest, vol. III, pp. 1301-1304.

13. Neal Erickson personal communication.

14. Antti Raissanen personal communication.

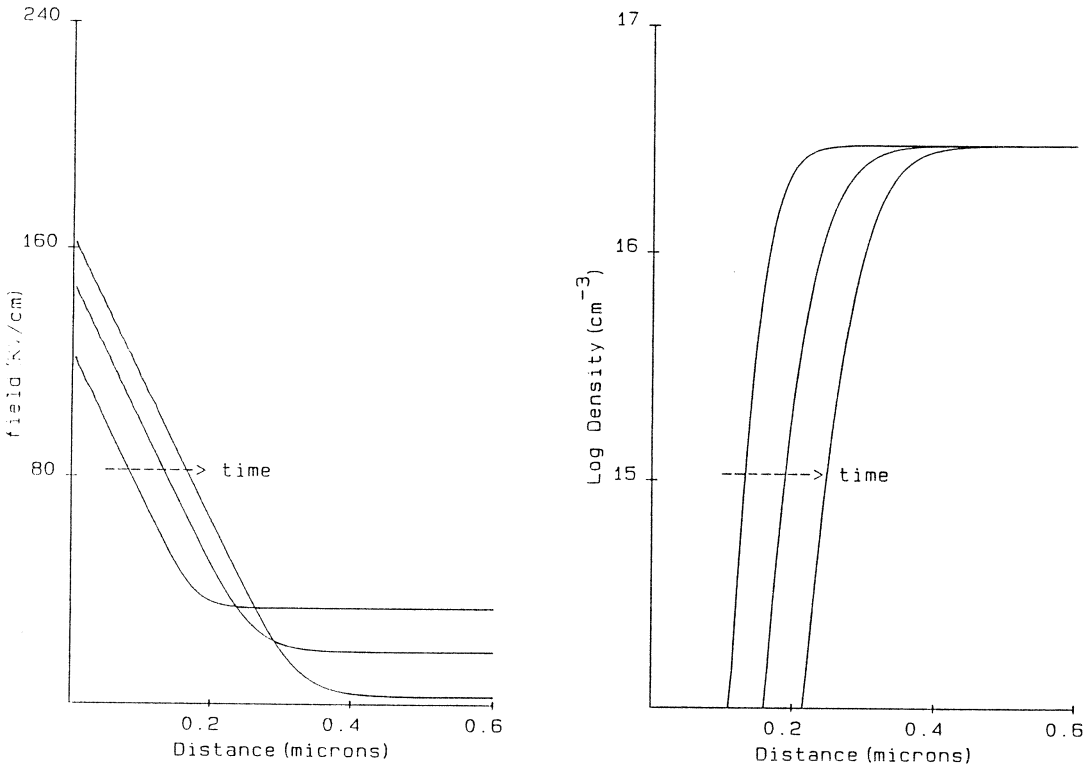

Figure 1

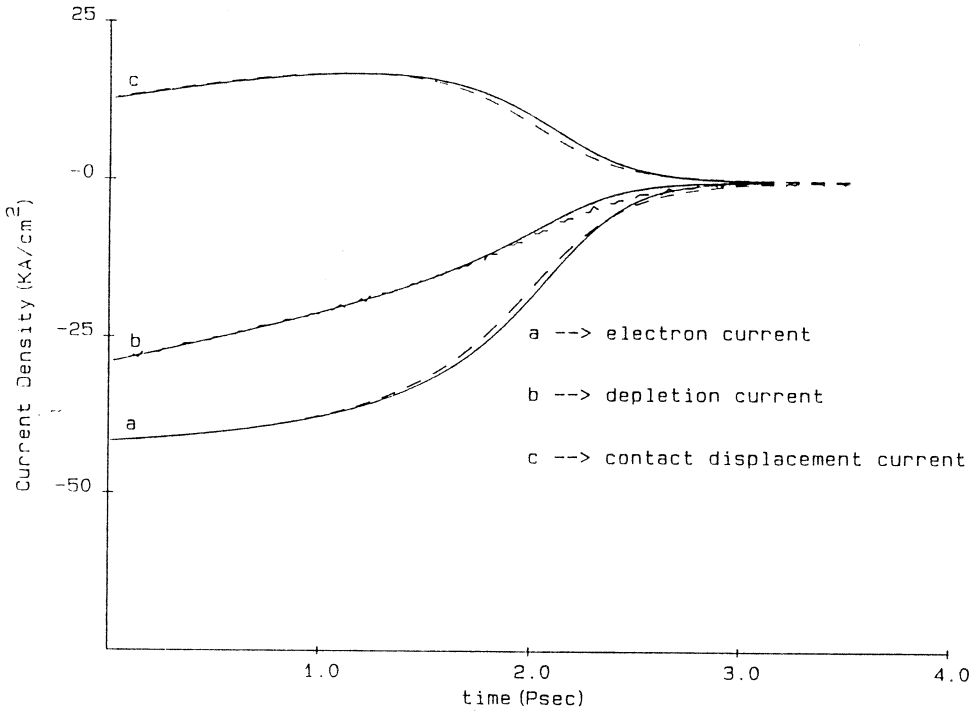

Figure 2

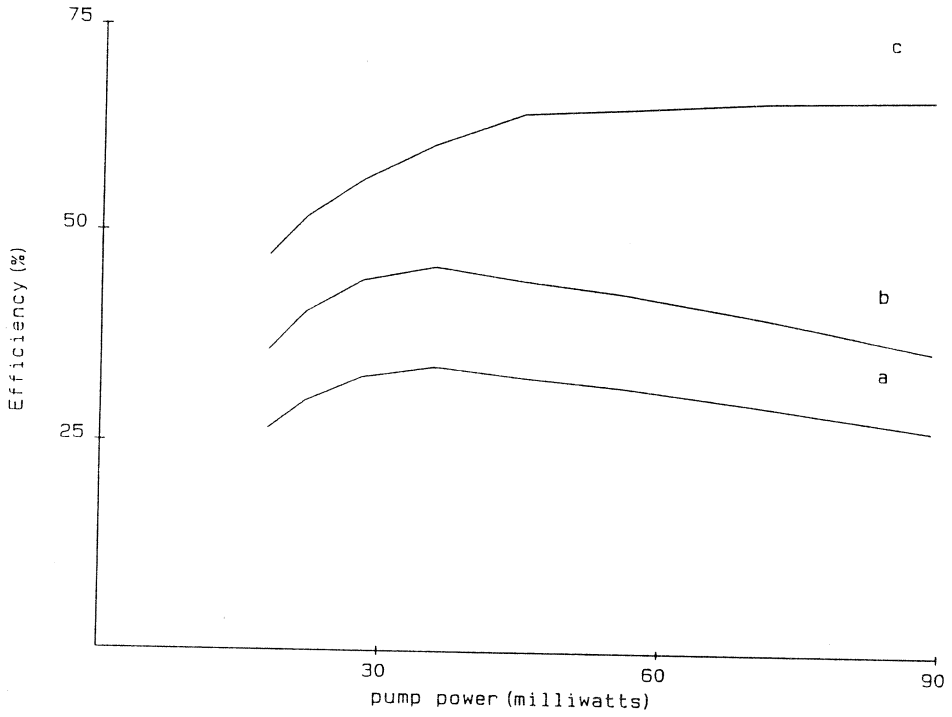

Figure 3

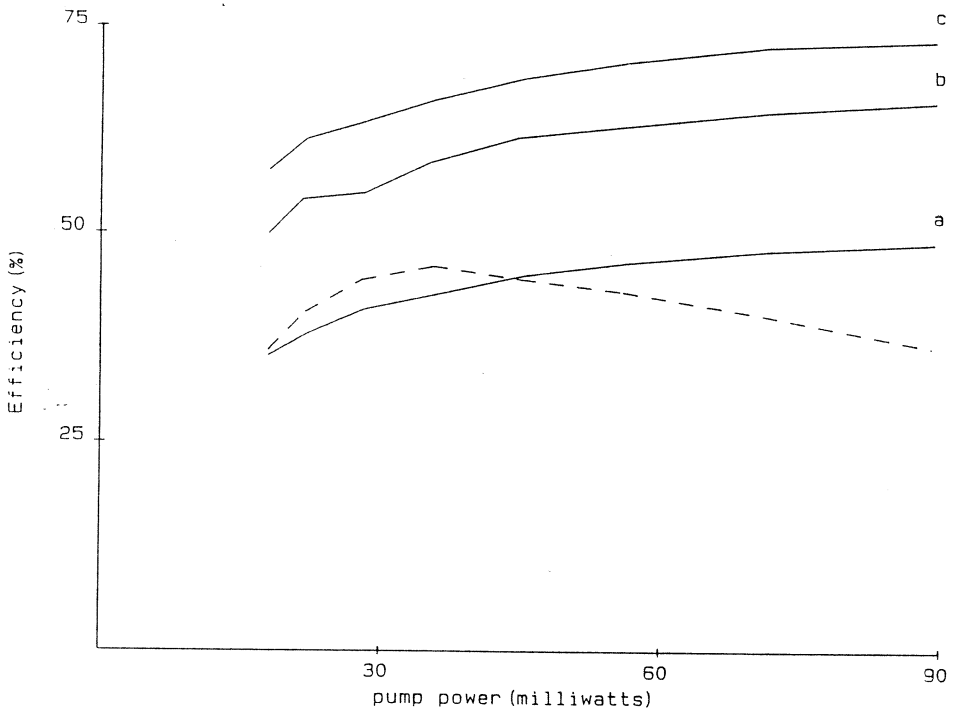

Figure 4

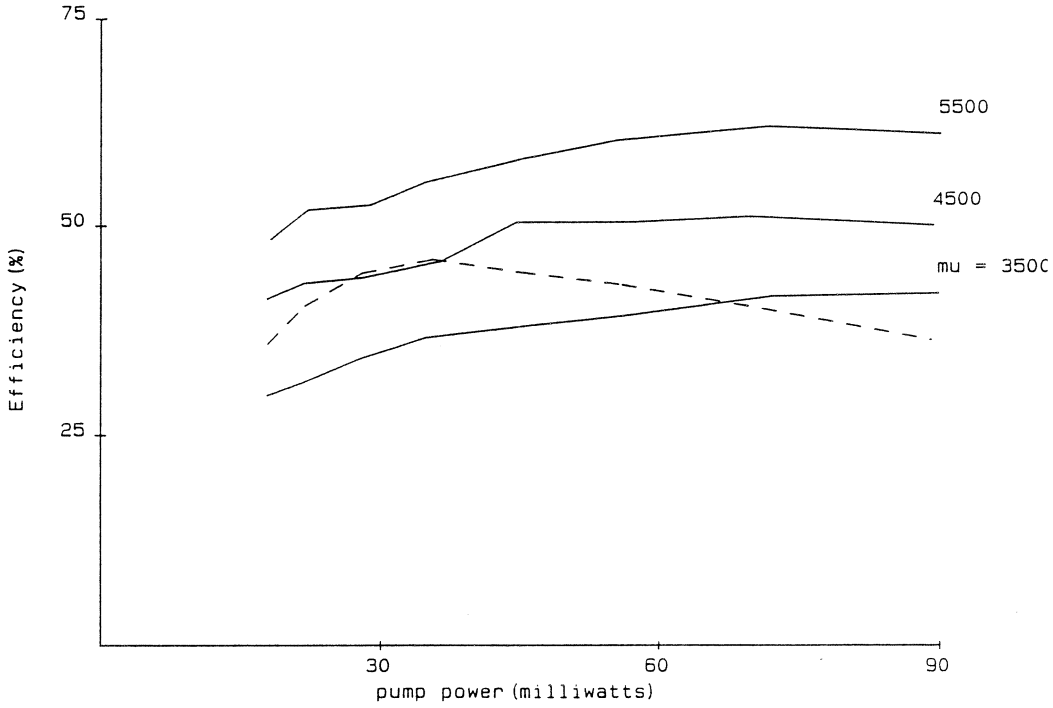

Figure 5

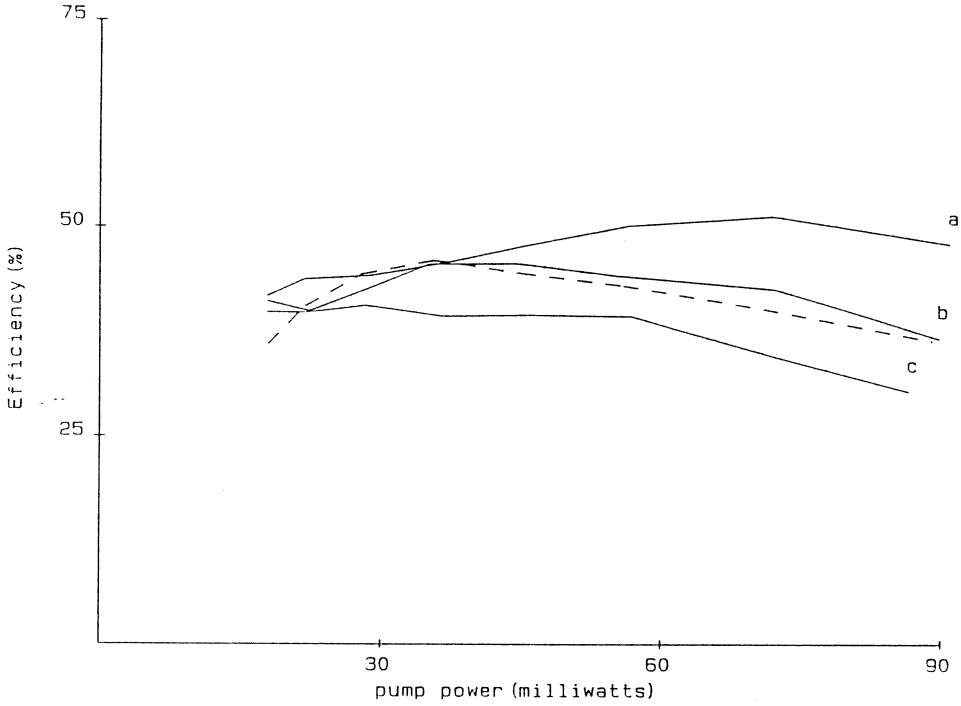

Figure 6

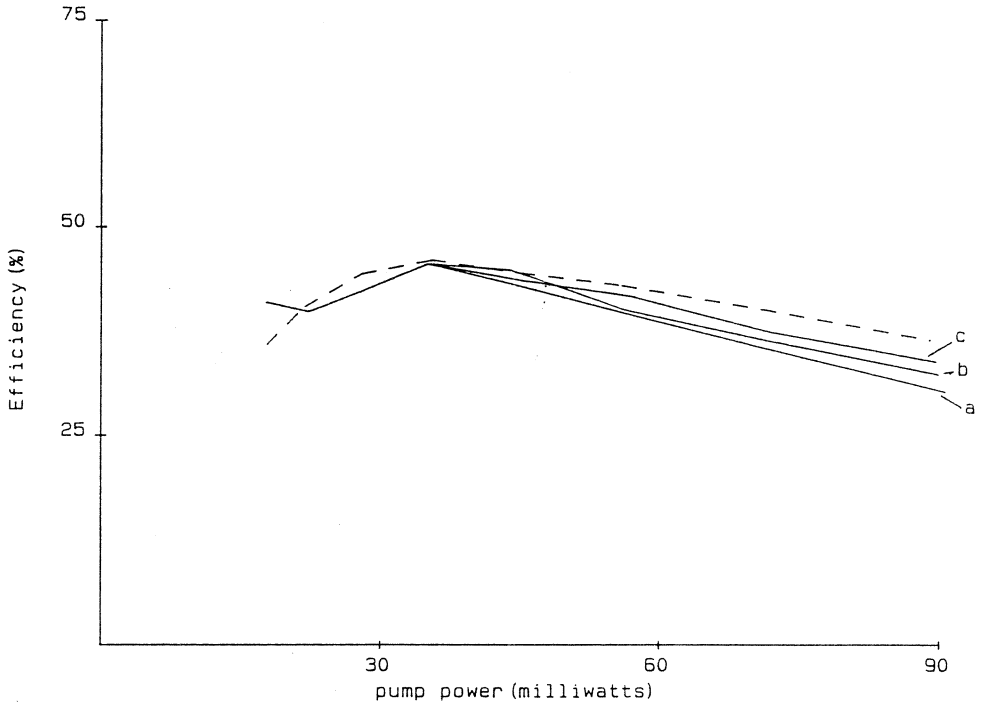

Figure 7